Faraday Discuss. Chem. Soc., 1986, **82**, 79–88

Photodissociation Dynamics of ICN

Unequal Population of the CN $X^2\Sigma^+$ Fine-structure Components

H. Joswig, Maureen A. O'Halloran and Richard N. Zare

Department of Chemistry, Stanford University, Stanford, California 94305, U.S.A.

Mark S. Child

Department of Theoretical Chemistry, Oxford University, 1 South Parks Road, Oxford OX1 3QZ

Photolysis of ICN at 281.5, 266 and 249 nm produces CN $X\ ^2\Sigma^+$ fragments in which the population of the $F_1(J''=N''+\frac{1}{2})$ and $F_2(J''=N''-\frac{1}{2})$ fine-structure components vary markedly as a function of v'', N'' and dissociation wavelength. Population differences favour either F_1 or F_2, and can be $>2:1$. A model is proposed to explain this behaviour, in which out-of-plane, spin-dependent forces cause the electron spin on CN to have a preferred orientation with respect to rotation of the CN fragment. The strong N'' dependence of the F_1/F_2 ratio is attributed to interference between different dissociation channels, probably enhanced by various curve crossings.

1. Introduction

Internal state distributions of photofragments are often a sensitive probe of the dynamics which characterize a specific photodissociation process. Perhaps the best known examples involve the distributions of rotational and vibrational energy in the fragments, from which mechanisms for partitioning of the excess energy of dissociation can be deduced. A more subtle example is the unequal population of the nearly degenerate Λ-doublet levels of a $^2\Pi$ molecular fragment, such as those produced in the photodissociation of NH_3[1,2], H_2O[3,4] and HONO.[5,6] In these cases the population difference of the Λ-doublet states can be interpreted in terms of the geometrical arrangement of the π-electron lobe relative to the rotation of the fragment. The case of a $^2\Sigma$ molecule is even more interesting. Each rotational level, N, is split by coupling of the spin of an unpaired electron to rotation to form the two components, F_1 and F_2, characterized by total angular momentum $J=N+\frac{1}{2}$ and $J=N-\frac{1}{2}$, respectively. There is no geometrical reason to expect a difference between the populations of the two levels other than that given by the $2J+1$ statistical weighting factor. Nonetheless, Wittig and coworkers[7-9] have recently reported an unequal population of the F_1 and F_2 components of the CN $X\ ^2\Sigma^+$ fragment produced in the photodissociation of the ICN and BrCN at 266 nm. In these cases the explanation for the population difference must involve the complicated electronic structure of the molecules, rather than simple geometrical arguments. Several excited states, leasing asymptotically to the two different exit channels which produce $I(^2P_{3/2})$ or $I^*(^2P_{1/2})$, are known[10] to be involved in the photodissociation of the ICN. In addition, measurements of the alignment and the angular distribution of the CN fragments suggest a strong mixing of the states involved.[9,11-13]

In this paper we present detailed experimental results concerning the anomalous population of the spin-rotation states in the CN $X\ ^2\Sigma^+$ fragment produced in the photodissociation of ICN. Three different photolysis wavelengths (249, 266 and 281.5 nm) are used, covering different portions of the so-called $\tilde{A}$ absorption continuum of ICN. According to the results of Pitts and Baronavski,[10] the photodissociation

dynamics should be sensitive to the contributions of different electronic states to the $\tilde{A}$ absorption continuum as the wavelength is changed. A model is presented to explain the preferential population of the F_1 and F_2 components for a $^2\Sigma$ photofragment and the observed variation of population differences as a function of the final rotational quantum number N.

2. Experimental

ICN (Eastman-Kodak) was purified by resublimation and its vapour was made to flow slowly through a vacuum chamber, typically at pressures of 5–20 mTorr. The ICN molecules were photodissociated by u.v. laser pulses at 249, 266 or 281.5 nm, and the CN $X\ ^2\Sigma^+$ fragments were then detected *via* laser-induced fluorescence by a probe dye laser tuned through the CN $B\ ^2\Sigma^+$–$X^2\Sigma^+$ transition. The two laser beams entered the chamber collinearly and anti-parallel, and fluorescence was collected with a lens normal to the propagation direction of both lasers and imaged onto a photomultiplier tube (RCA 7326). Light baffles and a filter act to suppress scattered light. The photomultiplier signal was processed by a boxcar integrator (EG&G PAR, models 162 and 165) and displayed on a chart recorder.

Several laser systems were used to generate the different photodissociation wavelengths. An excimer laser (Lumonics TE 861) with a KrF gas mixture provide a photolysis wavelength of 249 nm. Light of 266 nm was provided by the fourth harmonic of an Nd:YAG laser (Quanta Ray DCR-1, HG-2). For 281.5 nm, the frequency-doubled output of an Nd:YAG pumped dye laser (Quantel 581C) was employed. In each case the dissocation pulses were 10 ns long, and the output was unfocused and limited to 5–20 mJ per pulse.

The excimer laser at 249 nm is also used to pump a probe dye laser (Lambda Physik FL2002E), which was operated at low power (without the second amplification stage) in order to avoid saturation effects. The bandwidth of the laser was *ca.* 0.2 cm^{-1}, and could be narrowed to *ca.* 0.04 cm^{-1} by use of an intracavity etalon. Scanning was accomplished by a combination of angle and pressure tuning. The delay between the pump and probe lasers could range from 0 to 400 ns; in all cases, the delay and the ICN pressure were chosen to establish collision-free conditions, so that it was the nascent CN $X\ ^2\Sigma^+$ fragment distribution that was being determined. The signals were confirmed to be linear with respect to ICN pressure and to dissociation and probe laser powers.

In a separate experiment the polarization dependendence of the signals was measured.[13] It should be emphasized that the polarization dependence of the signals was the same for the F_1 and F_2 components, and the signal difference reflects a population difference and not an alignment effect.

3. Results

We observe unequal populations of the F_1 and F_2 components in the CN $X\ ^2\Sigma^+$ fragment for all the vibrational levels $v'' = 0, 1, 2$ examined. In the lower vibrational levels $v'' = 0, 1$, however, a considerable amount of the excess energy is channelled into translation, leading to Doppler broadening of the lines and prohibiting the resolution of the spin-rotation components at lower N''. Wittig *et al.*[9] have used a different experimental technique based on lineshape measurements in two geometries and a lineshape fitting procedure in order to overcome this problem. We concentrate here on the vibrational state $v'' = 2$, for which it is possible to resolve directly the F_1 and F_2 components over a large range of N''.

Fig. 1 shows a 'low resolution' scan of a portion of the CN $B\ ^2\Sigma^+$–$X\ ^2\Sigma^+$ (0, 2) band. Although the two spin-rotation components are not completely resolved, it is obvious that the F_1 and F_2 levels are unequally populated. Fig. 2 shows a 'high-resolution' scan

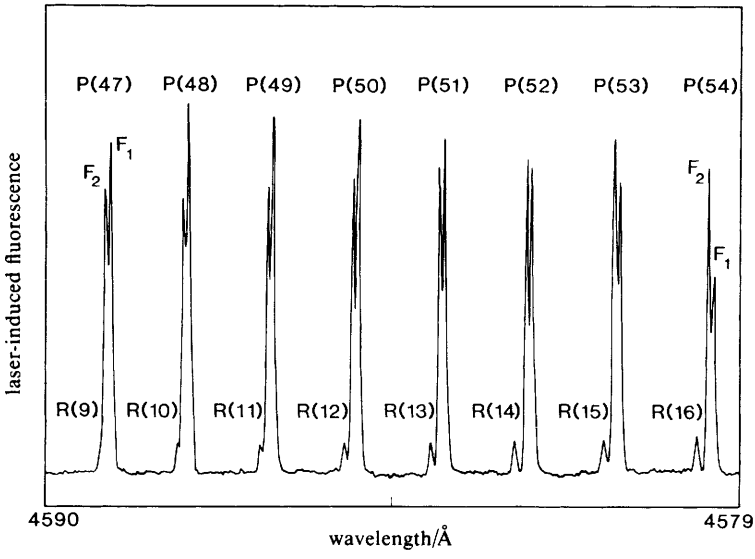

Fig. 1. Portion of the CN $B\,^2\Sigma^+ - X\,^2\Sigma^+$ (0, 2) fluorescence excitation spectrum following photolysis of ICN at 249 nm. Unequally populated F_1 and F_2 components are observed for high N''.

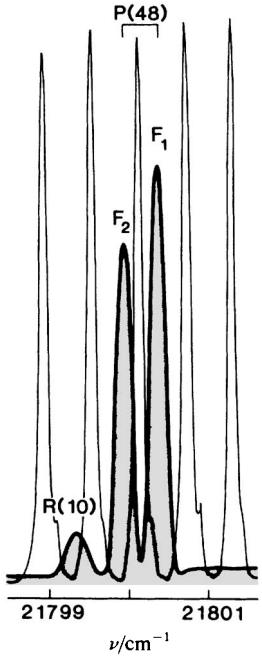

Fig. 2. High-resolution fluorescence excitation spectrum of the P(48) line shown in fig. 1. The shaded area represents the fluorescence signal; the background fringes are produced by a monitor etalon ($\Delta\nu \approx 0.61$ cm^{-1}). The probe laser bandwidth is *ca.* 0.04 cm^{-1}.

over the P(48) line. Here, the F_1 and F_2 levels are resolved and the difference in population can be clearly determined. The relative populations for the two fine-structure components have been determined from such 'high-resolution' scans for as many rotational elvels as could be resolved for each of the different dissociation energies.

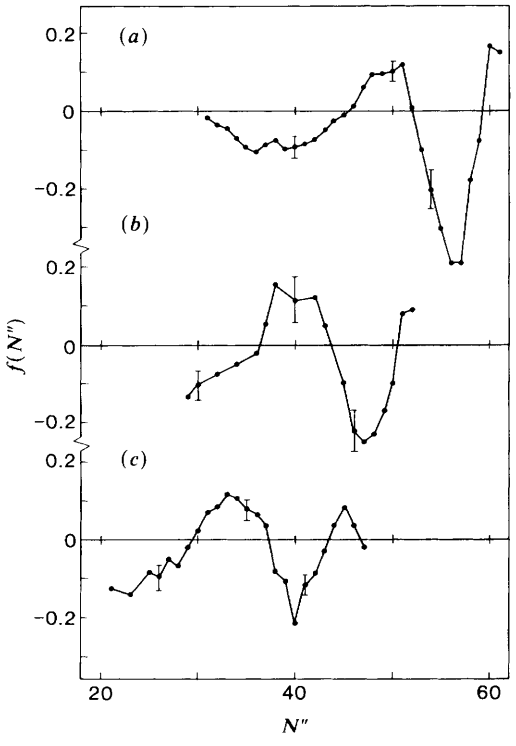

Fig. 3. The fine-structure difference function $f(N'')$ *vs.* N'' for photolysis of ICN at (*a*) 249, (*b*) 266 and (*c*) 281.5 nm. Representative error bars are indicated.

In fig. 3 we plot the quantity

$$f(N'') = [n(F_1) - n(F_2)]/[n(F_1) + n(F_2)] \tag{1}$$

where $n(F_{1,2})$ represents the population in the F_1 or F_2 levels, respectively, for the same values of N''. $f(N'')$ is shown as a function of final CN rotational quantum number, N'', for the three different dissociation wavelengths. $f(N'')$ exhibits a strong N'' dependence with an oscillatory behaviour, favouring F_1 over F_2 for certain N'', where for other values of N'', F_2 is dominant. For each dissociation wavelength, the highest observed levels, N''_{max}, is close to the highest value allowed by conservation of energy. Hence the shifts of N''_{max} by 15 units from fig. 3(a) to (*b*) and by 23 units from fig. 3(*a*) to (*c*) are accounted for by the change in excitation wavelengths. The function $f(N'')$ thus seems to depend principally on $N''_{max} - N''$, so that the above shifts bring the three diagrams essentially into coincidence when $f(N'')$ is plotted on a scale linear with N''. In the following section we offer a model to account qualitatively for the existence of the spin-rotation population differences and for their variation with dissociation energy and N''.

4. Theory

Fig. 4 introduces the angular momenta involved, defined for nearly separated fragments: $\boldsymbol{j}$, the total electronic angular momentum of the iodine atom ($j = \frac{1}{2}$ or $\frac{3}{2}$); $\boldsymbol{S}$ the electronic spin of the CN radical ($S = \frac{1}{2}$); $\boldsymbol{N}$, the rotational angular momentum of CN ($N = 0, 1, 2, \ldots$); and $\boldsymbol{l}$ the orbital angular momentum of the recoiling fragments ($l = 0, 1, 2, \ldots$). Because the torque produced in ICN photodissociation is directed nearly

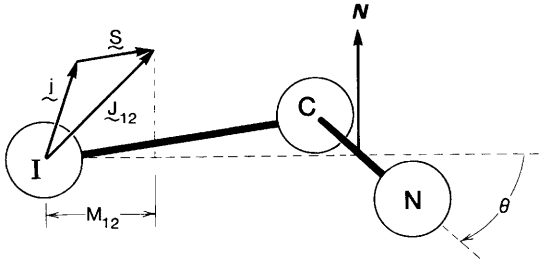

Fig. 4. Angular momenta describing the dissociation of ICN.

in the ICN plane, $\boldsymbol{N}$ points almost perpendicular to this plane and passes through the CN centre of mass. We assume that when the fragments are close together, spin–orbit interaction causes $\boldsymbol{j}$ and $\boldsymbol{S}$ to be coupled strongly to form the resultant $\boldsymbol{J}_{12}=\boldsymbol{j}+\boldsymbol{S}$. Moreover, we suppose that $\boldsymbol{J}_{12}$ is quantized with respect to the axis passing from the I atom through the CN centre of mass, giving rise to well defined components $\Lambda_{12}\equiv M_{12}$. On the same axis, which we take as the z axis in the molecular frame, $\boldsymbol{N}$ makes the projection M_N, where $M_N \ll N$.

Quantization along the I—C axis would be more realistic, but this would severely complicate what follows, and the I—C vector would still lie on average along the z axis. One might also argue that the orbital part of $\boldsymbol{j}$ should be at least partially quenched in the molecular region, but the following argument would still hold with $\boldsymbol{j}$ replaced by the electron spin on I, provided spin–orbit coupling was strong enough to cause the appearance of states with well defined M_{12}.

The Hamiltonian consistent with fig. 4 may be written as

$$H = H_0 + l^2/2\mu R^2 \tag{2}$$

where μ is the reduced mass of the CN and I fragments, R is their separation and H_0 is assumed to have eigenstates $|(jS)J_{12}N;\ M_{12}M_N\rangle \equiv |M_{12}, M_N\rangle$, *i.e.* CN is already rotating freely. Let us denote the total angular momentum of the excited ICN molecule as $\boldsymbol{J}_T=\boldsymbol{l}+\boldsymbol{N}+\boldsymbol{J}_{12}$. We can restrict the discussion to rotationally cold ICN ($J_T \approx 0$), since it is known that the rotation of the parent ICN has negligible effect on the distribution of rotational energy in the CN fragment. Then

$$\boldsymbol{l}+\boldsymbol{N}+\boldsymbol{J}\approx 0 \tag{3}$$

and upon substituting $-(\boldsymbol{N}+\boldsymbol{J}_{12})$ for $\boldsymbol{l}$ in eqn (2) it is seen that a coupling term

$$H' = \boldsymbol{N}\cdot\boldsymbol{J}_{12}/\mu R^2 \tag{4}$$

is obtained. The term H' is treated as a perturbation to H_0, and taken to be the non-adiabatic coupling term operating at a curve crossing between two potential-energy surfaces to cause the state $|M_{12}, M_N\rangle$ to develop amplitudes $p_\pm$ in the channels $|M_{12}\pm 1, M_N \mp 1)$, respectively. In essence, the $\boldsymbol{N}\cdot\boldsymbol{J}_{12}$ coupling term represents forces not directed in the I—CN scattering plane, and these forces cause non-adiabatic transitions between different potential curves denoted by M_{12}. Propagation of the excited state on the different potential-energy surfaces then give rise in the asymptotic region to the final superposition state:

$$|f\rangle = \sum_{v=-1}^{1} p_v \exp(i\phi_v)|M_{12}+v,\ M_N - v\rangle \tag{5}$$

where the phases ϕ_v arise from the evolution along the potential curves associated with different M_{12} values. Since $\boldsymbol{N}$ is related to $\boldsymbol{l}$ through eqn (3), the centrifugal contribution

Table 1. Non-zero coefficients $C(J_{12}, M_{12}; J, m_j, M_J)$ in the limits $N \gg 0$, $M_N \ll N$

J	J_{12}	$m_j = M_{12}+\frac{1}{2}$ $M_J = M_N-\frac{1}{2}$	$m_j = M_{12}+\frac{1}{2}$ $M_j = M_N-\frac{1}{2}$
$N+\frac{1}{2}$	$j+\frac{1}{2}$	$-[(J_{12}-M_{12})/4J_{12}]^{1/2}$	$-[(J_{12}+M_{12})/4J_{12}]^{1/2}$
$N-\frac{1}{2}$	$j+\frac{1}{2}$	$[(J_{12}-M_{12})/4J_{12})]^{1/2}$	$-[(J_{12}+M_{12})/4J_{12}]^{1/2}$
$N+\frac{1}{2}$	$j-\frac{1}{2}$	$-[(J_{12}+1+M_{12})/4(J_{12}+1)]^{1/2}$	$[(J_{12}+1-M_{12})/4(J_{12}+1)]^{1/2}$
$N-\frac{1}{2}$	$j-\frac{1}{2}$	$[(J_{12}+1+M_{12})/4(J_{12}+1)]^{1/2}$	$[(J_{12}+1-M_{12})/4(J_{12}+1)]^{1/2}$

to ϕ_v might be expected to vary with N even if the amplitudes p_v were relatively insensitive to N. Also important is the fact that trajectories that lead to different final values of N will sample different portions of the potential-energy surface.

We have concentrated here on the coupling term $\boldsymbol{N}\cdot\boldsymbol{J}_{12}$ and neglected other coupling terms (such as Coriolis terms that arise, for example, if $\boldsymbol{J}_T$ is non-zero). However, the main point is the presence of the above discussed non-adiabatic transitions and the form of the final superposition state [eqn (5)], regardless of the specific form of the coupling terms.

It remains to decompose the final state $|f\rangle$ into the detectable asymptotic states $|j(SN)J; m_jM_J\rangle$ with $\boldsymbol{S}$ recoupled to $\boldsymbol{N}$ to form the resultant $\boldsymbol{J}$. Straightforward angular momentum algebra shows that

$$\begin{aligned}|(jS)J_{12}N; M_{12}M_N\rangle &= \sum_{m_j,M_S}\langle jSm_jM_S|J_{12}M_{12}\rangle|jm_J\rangle|SM_S\rangle|NM_N\rangle \\ &= \sum_{m_j,M_S}\sum_{J,M_J}\langle jSm_jM_S|J_{12}M_{12}\rangle\langle SNM_SM_N|JM_J\rangle|j(SN)J; m_jM_J\rangle \\ &= \sum_{J,M_J,m_i}[(2J_{12}+1)(2J+1)]^{1/2}(-1)^{N-J+M_{12}+M_J} \\ &\quad\times\begin{pmatrix} j & J_{12} & S \\ -m_j & M_{12} & -M_S\end{pmatrix}\begin{pmatrix} N & J & S \\ M_N & -M_J & M_S\end{pmatrix}|j(SN)J; m_jM_J\rangle.\end{aligned} \tag{6}$$

Since $S=\frac{1}{2}$, the sum in eqn (6) is limited for fixed j and J_{12} to two terms with (m_j, M_J) equal to $(M_{12}+\frac{1}{2}, M_N-\frac{1}{2})$ or $(M_{12}-\frac{1}{2}, M_N+\frac{1}{2})$ for each of the possible values of $J=N+\frac{1}{2}$ or $J=N-\frac{1}{2}$. Table 1 collects the coefficients for the different $|(jS)J_{12}N; M_{12}M_N\rangle$ appearing on the right-hand side of eqn (6) in the limits $N\gg 0$ and $N\gg M_N$. The most important feature of these coefficients for the present discussion is that the relative signs of the two entries for given J_{12} and N differ according to whether $J=N+\frac{1}{2}$ or $J=N-\frac{1}{2}$.

The quantity experimentally measured is the probability for the CN fragment to be in one of two J levels for a given value of N. This is given by

$$P(N,J)=\sum_{m_j,M_J}|\langle j(SN)J; m_jM_J|f\rangle|^2 \tag{7}$$

and it is readily verified by use of table 1 that the ratio of spin-rotation component populations is

$$\begin{aligned}\frac{P(F_1)}{P(F_2)} &= \frac{P(N, J=N+\frac{1}{2})}{P(N, J=N-\frac{1}{2})} \\ &= \frac{X_+ \pm 2p_0p_+\lambda_+\cos(\phi_0-\phi_+)\pm 2p_0p_-\lambda_-\cos(\phi_0-\phi_-)}{X_+ \mp 2p_0p_+\lambda_+\cos(\phi_0-\phi_+)\mp 2p_0p_-\lambda_-\cos(\phi_0-\phi_-)}\end{aligned} \tag{8}$$

where

$$X_+ = 2J_{12}p_0^2+(J_{12}-M_{12}+1)p_-^2+(J_{12}+M_{12}+1)p_+^2 \tag{9}$$

$$X_- = (2J_{12}+2)p_0^2 + (J_{12}-M_{12})p_+^2 + (J_{12}+M_{12})p_-^2 \tag{10}$$

$$\lambda_\pm = [J_{12}(J_{12}+1) - M_{12}(M_{12}\pm 1)]^{1/2} \tag{11}$$

and the upper and lower signs in eqn (8) and (11) apply for $J_{12} = j+\frac{1}{2}$ and $J_{12} = j-\frac{1}{2}$, respectively. In the limits $p_\pm^2 \ll p_0^2$ and $p_p \approx 1$, the factors $X_\pm$ becomes $2j+1$.

Inspection of eqn (8)–(11) shows that the population ratio is independent of the sign of M_{12}, provided only that transitions from M_{12} to $M_{12}+1$ occur with equal facility as transitions from $-M_{12}$ to $-M_{12}-1$. Eqn (8) also shows that the departure of the spin-rotation population ratio $P(F_1)/P(F_2)$ from unity increases as the value of J_{12} becomes larger and that of M_{12} smaller, owing mathematically to the $\lambda_\pm$ factors in eqn (8) and physically to the larger projection of $\boldsymbol{J}_{12}$ onto $\boldsymbol{N}$ (see fig. 4). Conversely, $\lambda_+ = \lambda_- = 0$ for $J_{12} = 0$. Thus one would not expect a population preference to appear in the F_1, F_2 fine-structure components of a $^2\Sigma$ photofragment unless the companion photofragment has $j \neq 0$ and strong spin–orbit interaction causes $\boldsymbol{j}$ to be quantized along the separation axis. For example, one would anticipate no preference in the direction of the spin, relative to either rotation or orbital angular momentum, in either pair of photofragments for photodissociation of HCN or CH_3CN, but it might occur in the photodissociation of CH_3I or HI.[3]

As long as there is more than one surface correlating asymptotically to the same experimentally observable final state, there is the possibility of interference between the different pathways. The exact phase difference accumulated on the different possible paths will depend on both the particular trajectories followed and upon the distribution of probability between the different possible paths. The potential-energy surface that describes the interaction between the department fragments is a multidimensional surface. Even for the simple case of scattering between an atom and a rigid rotor, the potential energy still depends upon both the distance, R, between the two fragments and the angle, θ, between the axis of the diatom and the coordinate R. Which trajectories are followed on the potential-energy surfaces, and hence the differences in accumulated phase, will be dependent upon both the linear velocity, $\mathrm{d}R/\mathrm{d}t$, *i.e.* upon the excess energy, and upon the angular velocity, $\mathrm{d}\theta/\mathrm{d}t$, *i.e.* upon the rotational energy. Moreover, the crossings between these surfaces will not be single points, but rather seams, and the curve-crossing probability will vary depending on the difference in slope between the surfaces at different points along the seam and upon the velocity (excess energy) of the fragments. Thus the presence of a population difference which varies with both dissociation energy and with the final rotational state of the CN fragment can be easily understood.

5. Model Calculation

To complete this treatment, we calculate the spin-rotation population ratio using a simple semiclassical approach. The phase difference $\phi_0 - \phi_\pm$ are evaluated by integrating the momentum along the classical trajectory, so that

$$\phi_v = \lim_{R\to\infty} \int (\boldsymbol{k} - \boldsymbol{k}^\circ) \cdot \mathrm{d}\boldsymbol{R} \tag{12}$$

where the radial (R) and angular (θ) components of $\boldsymbol{k} = \boldsymbol{p}/\hbar$ are obtained by running a trajectory over the effective potential $V_v(R,\theta) + l(l+1)\hbar^2/2\mu R^2 + BN(N+1)$. In the calculation of $\boldsymbol{k}^\circ$ the potential $V_v(R,\theta)$ is omitted. The potentials are taken from Marinelli *et al.*[14] where we assign $V_0 = V_1$ and $V_\pm = V_3$. They obtained these potentials by fitting them to match the ICN absorption spectrum and the rotational distributions of the CN fragment produced following photodissociation of ICN at several photolysis wavelengths. Classical trajectories with initial conditions reflecting cold ICN are run

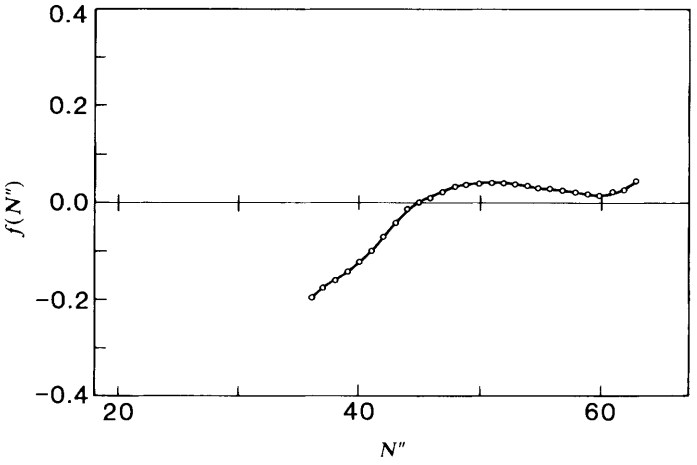

Fig. 5. Calculated fine structure difference function $f(N'')$ *vs.* N'' for photolysis of ICN at 249 nm, based on potential surfaces of Marinelli *et al.*[14]

on these surfaces, and phases are accumulated after passing through a curve crossing between the two potential-energy surfaces.

The parameters in eqn (8)-(11) are taken to be $j=\frac{3}{2}$, $J_{12}=2$, and $M_{12}=0$. With $M_{12}=0$, there is no difference between the $M_{12}=+1$ and $M_{12}=-1$ coupling, and $\lambda_+=\lambda_-$, $p_+=p_-$ and $\phi_+=\phi_-$. We use the values $p_0=0.94$ and $p_+=p_-=0.25$, and $B=1.8563\ \mathrm{cm}^{-1}$. Fig. 5 shows results of this calculation, displayed in the same way as the experimental data in fig. 3, namely, as $f(N'')$ *vs.* N''. The model is considered to be only qualitatively correct: the full average over different excited states, *e.g.* the intercontinuum coupling between different vibrational levels, has not been taken into account. The calculations do show, however, that a relatively small curve crossing probability is sufficient to give spin-rotation population differences of the same order of magnitude as observed. Moreover, the accumulated phase changes with N'' in such a manner as to cause a reversal of this preference.

An even simpler model can be adopted in which the curve crossing is assumed to occur at a distance, R, beyond the range of significant coupling between radial and angular motion. The phase terms then reduce to one-dimensional integrals, so that

$$\phi_v = \lim_{R\to\infty} \int_{R_x}^{R} \left(\frac{2\mu}{\hbar^2} [E - BN(N+1) - V_v(R)] - l(l+1)/R^2 \right)^{1/2} \mathrm{d}R. \qquad (13)$$

These integrals diverge as $R\to\infty$, but the differences between them remain constant provided that the $V_v(R)$ have the same asymptotic limit.

Calculations have been made using two curves; $V_0(R)$, taken as the collinear section through the surface V_1 of Marinelli *et al.*,[14]

$$V_0 = V_{\mathrm{lim}} + 1.53\times10^8\ \mathrm{cm}^{-1} \exp(-3.5\text{Å}^{-1}R) \qquad (14)$$

and $V_-(R)$, taken in the Morse form,

$$V_-(R) = V_{\mathrm{lim}} + D_e \{\exp[-10\ \text{Å}^{-1}(R-R_e)] - 2\exp[-5\ \text{Å}^{-1}(R-R_e)]\} \qquad (15)$$

because it proved impossible to obtain sufficiently rapid variation in the relative population function, $f(N'')$, with a purely repulsive potential. The parameters adopted were $D_e=2706\ \mathrm{cm}^{-1}$, $R_e=3.622$ Å, and $V_{\mathrm{lim}}=3031\ \mathrm{cm}^{-1}$, which gives a curve crossing at $R_x=3.475$ Å. These parameters were chosen to fit the experimental data at 249 nm, subject to the constraint that the crossing point R_x be classically accessible at the highest

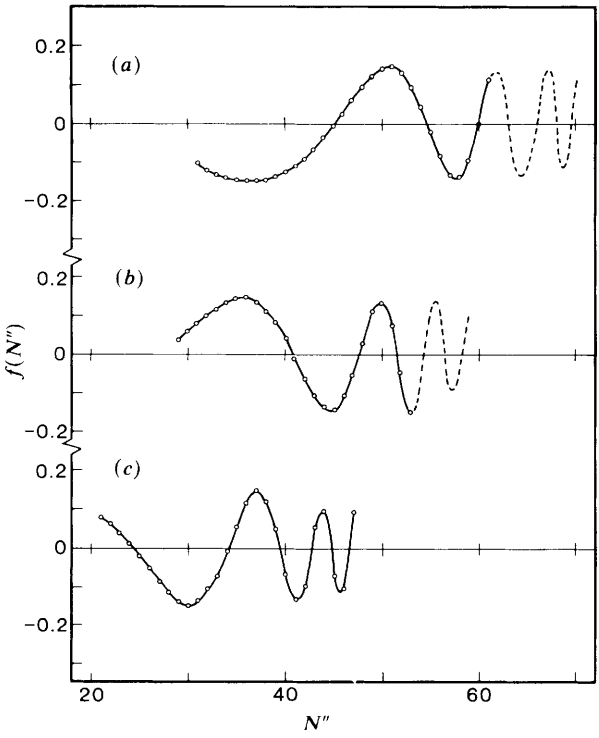

Fig. 6. Calculated fine-structure difference function $f(N'')$ *vs.* N'' for photolysis of ICN at (*a*) 249, (*b*) 266 and (*c*) 281.5 nm. One-dimensional potential-energy functions are used. Open circles represent values of N'' for which $f(N'')$ was measured.

observed value of N'', $N''_{max} = 47$, at lowest dissociation energy, when $\lambda = 281.5$ nm. The parameters of eqn (9) and (13)-(15) were $J_{12} = 2$, $M_{12} = 0$, $p_+ = 0$, $p_- = 0.5$ and $p_0 = 0.97$.

The continuous curves in fig. 6 cover the experimentally observed range indicated in fig. 3, and it is seen that the data for $\lambda = 249$ nm are indeed well reproduced, at least for $N'' > 40$. It is also interesting to observe that in the dashed extensions, which cover all classsically allowed values at $R = R_x$, the three curves begin to reproduce the translational superimposition evident in the experimental data. Moreover, this appears to be no accident relating to the choice of excitation energy, because phase differences at the non-integer cutoff values of $N'' = N''_{max}$ are almost identical; $\phi - \phi_0 = 38.7$, 38.9 and 38.8 for $\lambda = 249$, 266 and 281.5 nm, respectively. This remarkable result can be understood to some extent by noting that

$$\phi_- - \phi_0 = \int_{R_x}^{\infty} [k_-(R) - k_0(R)]\,\mathrm{d}R$$

$$= \frac{(2\mu)^{1/2}}{\hbar} \int_{R_x}^{\infty} \frac{V_0(R) - V_-(R)}{2k(R)}\,\mathrm{d}R \qquad (16)$$

where $\bar{k}(R) = 0.5[k_-(R) + k_0(R)]$, because the second integral is dominated by the region $R \approx R_x$, where $\bar{k}(R) \to 0$ as $N'' \to N''_{max}$, and because the R dependence of $\bar{k}(R)$ is dominated in this region by variations in the $V_v(R)$, rather than variations in the term $l(l+1)/R^2$ in eqn (13).

If this behaviour carries over to more realistic situations with several coupled degrees of freedom, it suggests that the seam between the surfaces is close to the Franck–Condon

region, *i.e.* the region directly above the potential-energy well of the bound parent molecule, so that the maximum N'' value observed is also the maximum value classically allowed. The spin-rotation component preference, $f(N'')$, is thus shown to be a sensitive measure of the complex photodissociation dynamics that occur when more than one potential surface interacts.

This work was supported by the U.S. National Science Foundation under NSF PHY-85-06668. H.J. thanks the Deutsche Forschungsgemeinschaft for a postdoctoral fellowship.

References

1 F. Alberti and A. E. Douglas, *Chem. Phys.*, 1978, **34**, 399.
2 A. M. Quinton and J. P. Simons, *Chem. Phys. Lett.*, 1981, **81**, 214.
3 P. Andresen and E. W. Rothe, *Chem. Phys.*, 1983, **78**, 989.
4 P. Andresen, G. S. Ondrey, B. Titze and E. W. Rothe, *J. Chem. Phys.*, 1984, **80**, 2548.
5 R. Vasudev, R. N. Zare and R. N. Dixon, *Chem. Phys. Lett.*, 1985, **96**, 399.
6 R. Vasudev, R. N. Zare and R. N. Dixon, *J. Chem. Phys.*, 1984, **80**, 10.
7 I. Nadler, H. Reisler and C. Wittig, *Chem. Phys. Lett.*, 1984, **103**, 451.
8 F. Shokoohi, S. Hay and C. Wittig, *Chem. Phys. Lett.*, 1984, **110**, 1.
9 I. Nadler, D. Mahgerefteh, H. Reisler and C. Wittig, *J. Chem. Phys.*, 1985, **82**, 3885.
10 W. M. Pitts and A. P. Baronavski, *Chem. Phys. Lett.*, 1980, **71**, 395.
11 J. H. Ling and K. R. Wilson, *J. Chem. Phys.*, 1975, **63**, 101.
12 G. E. Hall, N. Sivakumar and P. L. Houston, to be published.
13 M. A. O'Halloran, H. Joswig and R. N. Zare, unpublished work.
14 W. J. Marinelli, N. Sivakumar and P. L. Houston, *J. Phys. Chem.*, 1984, **88**, 6685.

Received 13*th May*, 1986